A FUZZY SEGMENTATION-BASED APPROACH TO EXTRACTION OF COASTLINES FROM IKONOS IMAGERY

Yu Li, Jonathan Li and Yao Lu, Department of Geography and Environmental Management
University of Waterloo, Waterloo, Ontario

This paper presents a new approach to effective and accurate extraction of coastlines from commercial high-resolution satellite imagery. The approach is based on a fuzzy segmentation algorithm, which models segmentation of a colour image as a fuzzy c-partition and uses colour histogram analysis and a genetic algorithm to determine the number of clusters and optimal fuzzy c-partition, respectively. After segmenting the satellite image into homogenous regions based on colour similarity, the segmented regions are classified into water and land semiautomatically. Then, morphological operations are applied to filter noise in the classified images. The coastline is finally extracted from the filtered images by a delineation algorithm. The developed approach is tested by using 1 m resolution IKONOS pan-sharpened imagery. The effectiveness of the algorithm is demonstrated by the experimental results and accuracy evaluation.

Cet article expose une nouvelle approche pour extraire de manière efficace et précise les lignes de côte à partir d'images satellitaires commerciales à haute résolution. L'approche est fondée sur un algorithme de segmentation flou qui modélise la segmentation d'une image en couleurs comme une partition de couleurs floue et utilise une analyse de l'histogramme de couleurs et un algorithme génétique pour déterminer respectivement le nombre de groupements et la partition de couleurs floue optimale. Après la segmentation de l'image satellitaire en régions homogènes en fonction de la similarité des couleurs, les régions segmentées sont regroupées manuellement en classes d'eau et de terre. Puis, des opérations morphologiques sont appliquées pour filtrer les bruits dans les images classifiées. Les lignes de côte sont finalement extraites des images filtrées par un algorithme de délimitation. L'approche développée est vérifiée en utilisant des images IKONOS d'une résolution d'un mètre dont la netteté est maximisée. L'efficacité de l'algorithme est démontrée par l'évaluation des résultats expérimentaux et de la précision.

Yu Li
y62li@envmail.uwaterloo.ca

Jonathan Li
junli@uwaterloo.ca

Yao Lu
y25lu@envmail.uwaterloo.ca

1. Introduction

Coastline mapping and change detection are critical for various applications, ranging from coastline erosion and evolution monitoring, to sustainable coastal zone development and planning, coastal flood forecasting, and the potential effect of tsunamis on safety of navigation [*Green and King* 2003; *Polngam et al*. 2005; *Ruiz et al*. 2007; *Marfai et al*. 2008]. This task is difficult, time consuming, and sometimes impossible for a huge region such as an entire continent when using traditional ground survey techniques, in part because water bodies can be fast-moving (e.g. floods, tides, and storm surges) or may be inaccessible. Although tracing coastlines manually is easy along relatively simple stretches of a coast, it is not practical when coastlines become very complex. In addition, automatic and replicable techniques are required to update coastline maps, to evaluate the spatial and temporal evolution of alterations due to natural and anthropic events, and to extract the shoreline for large areas.

Today, several commercial Earth-observing satellites provide increasingly high-spatial-resolution multispectral images. These satellites normally bundle a 4:1 ratio of a high-resolution panchromatic (PAN) band and lower resolution multispectral (MS) bands in order to support both colour and best spatial resolution, while minimizing on-board data handling needs. For example, IKONOS and Orbview-3 both provide 1 m PAN (panchromatic) and 4 m MS (multispectral) images, QuickBird provides 0.6 m PAN, 2.4 m MS images, and the upcoming GeoEye-1 will provide 0.4 m PAN and 1.6 m MS images, all of which represent viable alternatives to high-resolution aerial imagery. It has been proven that the on-ground fusion of PAN and MS bands (namely, pan-sharpening) can provide an improved product to users, dependent upon the ability of the fusion technique to accurately reproduce fused imagery from multi-spectral imagery while improving the spatial resolution [*Zhang*

…studies have been carried out to develop digital image-processing techniques for detecting and delineating water bodies…from satellite multispectral images.

2004]. It has been found that automated tasks, such as feature extraction and segmentation/classification, benefit from pan-sharpening [*Wang et al*. 2005; *Colditz et al*. 2006]. Today, the pan-sharpening function is available with commercial remote-sensing software packages like PCI Geomatica, ERDAS Imagine, and ENVI.

Several studies have been carried out to develop digital image-processing techniques for detecting and delineating water bodies or coastlines from satellite multispectral images. In general, the existing coastline extraction methods can be grouped into two types: edge-based and segmentation-based. An example of an edge-based method for coastline extraction can be found in *Heene and Gautama* [2000], in which the Canny edge detector was used with a Gaussian kernel to smooth noise, to compute the edge strength and direction for each pixel in the smoothed image, and to identify the candidate edge. By a thinning process, the edge strength of each candidate edge pixel is set to zero if it is smaller than the edge strength of the two adjacent pixels in the gradient direction. Finally, the thinned edge magnitude image is set as a threshold. All candidate edge pixels above the threshold are marked as edge pixels.

Segmentation-based methods divide the image into homogeneous regions according to a given criterion, identify the major water and land regions, and generate an initial coastline as the boundary between water and land. An example of a segmentation-based method for coastline extraction can be found in *Li et al*. [2003], in which they attempted to improve IKONOS rational functions for better ground accuracy and to employ the improved rational functions for 3D coastline extraction using 1 m resolution PAN stereo images. Their study demonstrates that a coastline derived from IKONOS imagery can attain a ground accuracy of about 2-4 m, which is close to the NOAA/NGS (National Oceanic and Atmospheric Administration/National Geodetic Survey) 1:5,000 Coastal Topographic Survey Sheet (T-Sheet) accuracy, and higher than the accuracy of USGS (U.S. Geological Survey) 1:24,000 topographic maps. Researchers from the same unit [*Di et al*. 2003] developed a semi-automatic method to extract coastlines from IKONOS 1 m resolution PAN and 4 m resolution MS images. Their method is based on mean shift segmentation, major water body identification, initial shoreline extraction, and shoreline refinement. The accuracies of the extracted coastlines from 4 m MS and 1 m PAN stereo images are estimated to be 8.5 m and 2.3 m, respectively. *Liu and Jezek* [2004] proposed an image segmentation approach based on a locally adaptive thresholding technique, by which reliable results were achieved for the segmentation of a 30 m resolution Landsat-7 ETM+ band 5 image.

The main objectives of this study are: (1) to propose a new segmentation algorithm combining fuzzy c-partitioning, colour histogram analysis and genetic algorithms; and (2) to develop a coastline extraction approach based on the proposed segmentation algorithm. The paper is organized as follows: Section 2 gives the background, which explains the principle of the method. Section 3 details the proposed coastline extraction approach. Section 4 shows how this approach can be applied to coastline extraction from IKONOS pan-sharpened imagery. The accuracy assessment and conclusions are given in Sections 5 and 6, respectively.

2. Background

2.1 Fuzzy C-Partition

According to the fuzzy paradigm [*Klir and Yuan* 1995], fuzzy clustering can be seen as partitioning a data space into a number of fuzzy sets and assigning each data point a membership corresponding to each cluster. Consider a vector set V formed by n vectors in L dimensional real number space R^L, i.e., $V = \{\boldsymbol{v}_1, \ldots, \boldsymbol{v}_n\}$, $\boldsymbol{v}_j = (v_{j1}, \ldots, v_{jL}) \in R^L$ and $j = 1, 2, \ldots, n$, a fuzzy c-partition on V is represented by a fuzzy partition matrix P,

$$P = [p_{ij}],\ i = 1, \ldots, c \text{ and } j = 1, \ldots, n \tag{1}$$

where c is the number of clusters into which V is partitioned and the elements p_{ij} of P satisfy,

$$\sum_{i=1}^{c} p_{ij} = 1, \text{ for } j = 1, ..., n \tag{2}$$

$$0 < \sum_{j=1}^{n} p_{ij} < n, \text{ for } i = 1, ..., c \tag{3}$$

where $p_{ij} \in [0, 1]$ is the fuzzy membership of $\boldsymbol{v}_j$ belonging to the ith cluster. It is helpful to explain two issues before the design of the segmentation algorithm based on fuzzy c-partition: (1) how to determine the number of clusters c in the c-partition; and (2) how to obtain the optimal fuzzy c-partition-matrix. It is quite popular to assume that the number of clusters is known before designing the segmentation algorithm. However, it is difficult to specify the desired number of clusters, especially in the case of satellite image segmentation, since the ground truth is normally not available in advance. In this study, we use colour histogram analysis to determine the number of clusters and genetic algorithms to obtain

the optimal fuzzy c-partition matrix based on colour similarity measurement.

2.2 Vector Similarity

Consider a vector set V which is partitioned in c clusters. Each cluster in the fuzzy c-partition is assigned a centre vector defined in R^L, and all c centre vectors form a centre vector set $\boldsymbol{VC} = \{\boldsymbol{vc}_1, \boldsymbol{vc}_2, \ldots, \boldsymbol{vc}_c\}$. The fuzzy c-partition matrix can be calculated as follows [*Li et al*. 2005],

$$p_{ij} = \frac{\mu\left(\boldsymbol{v}_j, \boldsymbol{vc}_i\right)^{\frac{1}{m-1}}}{\sum_{k=1}^{c} \mu\left(\boldsymbol{v}_j, \boldsymbol{vc}_i\right)^{\frac{1}{m-1}}}, \text{ for } i = 1, ..., c \text{ and } j = 1, ..., n \tag{4}$$

where $m \in (1, \infty)$ is the weighting exponent for each fuzzy membership. The larger m is, the fuzzier the partition is. And $\mu(\boldsymbol{v}_j, \boldsymbol{vc}_i)$ is a similarity measure between vectors $\boldsymbol{v}_j$ and $\boldsymbol{vc}_i$ that can be calculated by

$$\mu(\boldsymbol{v}_j, \boldsymbol{vc}_i) = \exp\lfloor -k_1 d(\boldsymbol{v}_j, \boldsymbol{vc}_i) \rfloor \cos\lfloor k_2 \theta(\boldsymbol{v}_j, \boldsymbol{vc}_i) \rfloor \tag{5}$$

where k_1 and k_2 are parameters and $d(\boldsymbol{v}_j, \boldsymbol{vc}_i)$ and $\theta(\boldsymbol{v}_j, \boldsymbol{vc}_i)$ are the distance and the angle between $\boldsymbol{v}_j$ and $\boldsymbol{vc}_i$ defined by

$$d\left(\boldsymbol{v}_j, \boldsymbol{vc}_i\right) = \left(\sum_{l=1}^{L} \left| v_{jl} - vc_{il} \right|^2 \right)^{1/2} \tag{6}$$

$$\theta\left(\boldsymbol{v}_j, \boldsymbol{vc}_i\right) = \arccos\left(\frac{\sum_{l=1}^{L} v_{jl} vc_{il}}{\sqrt{\sum_{l=1}^{L} v_{jl} \sum_{l=1}^{L} vc_{il}^2}} \right) \tag{7}$$

2.3 Genetic Algorithms

Genetic algorithms are computer procedures that employ the mechanics of natural selection and natural genetics to evolve solutions to problems [*Goldberg* 1989]. Given a specific problem to solve, the input to genetic algorithms is a set of potential solutions to that problem, encoded in some fashion. A metric called a fitness function allows each candidate to be quantitatively evaluated. These candidates may be solutions already known to work, but more often they are randomly generated. In a pool of randomly generated candidates, promising candidates are kept and allowed to reproduce from each candidate evaluated according to the fitness function, using a series of genetic operations: selection, crossover and mutation.

There are many techniques which a genetic algorithm can use to select the individuals to be copied over into the next generation. Roulette-wheel selection is one of the most common methods. It is a form of fitness-proportionate selection in which the chance of a selected individual is proportional to the amount of its fitness. Conceptually, this can be described as a game of roulette: each individual gets a slice of the wheel, but fitter ones get larger slices than weaker ones. The wheel is then spun, and whichever individual owns the section on which the selection point lands each time is chosen. Once fit individuals have been chosen from several selections, they must be randomly altered in hopes of improving their fitness for the next generation. There are two basic strategies to accomplish this. The first and simplest one is called *mutation*. Just as mutation in living things changes one gene to another, so mutation in a genetic algorithm causes small alterations at a single point in an individual's code. The second method is called *crossover*, and entails choosing two individuals to swap segments of their codes, producing artificial offspring that are combinations of their parents. This process is intended to simulate the analogous process of recombination that happens in chromosomes during sexual reproduction. A common form of crossover is single-point crossover, in which a point of exchange is set at a random location in the two individuals' genomes: one individual contributes all its code from before that point, and the other contributes all its code from after that point to produce an offspring.

2.4 Colour Histogram

Colour histogram is an important technique in colour image analysis because of its efficiency, effectiveness and triviality in computation [*Pratt* 1991]. Generally speaking, a colour histogram represents the statistical distribution of the colours in an image [*Shapiro and Stockman* 2001].

…a colour histogram represents the statistical distribution of the colours in an image…

Given a colour space divided into I colour bins, the colour histogram of a colour image with n pixels is represented as a vector $H = [h_0, \ldots, h_{I-1}]$, in which each entry h_i indicates the statistics of the colours in the colour image which belong to the ith bin, i.e.,

$$h_i = \frac{n_i}{n}, \; i = 0, 1, ..., I - 1 \tag{8}$$

where n_i is the number of pixels with colours in the ith bin. Let the R, G, and B axes in the RGB colour space be divided into N_R, N_G, and N_B, which have equal length intervals in each axis. Then the total bins, N (= N_R x N_G x N_B) can be obtained. These bins are coded in the sequence from R to G and then to B. According to the specified discretizing

and coding scheme, the index of each bin can be expressed as

$$i = R + N_G \times G + N_B^2 \times B \quad (9)$$

where $R = 0, 1, \ldots, N_R - 1$, $G = 0, 1, \ldots, N_G - 1$, and $B = 0, 1, \ldots, N_B - 1$. Then the colour (r_p, g_p, b_p) will be in the bin with the index i_p, which can be expressed as,

$$i_p = \left\lfloor \frac{r_p N_R}{256} \right\rfloor + N_G \times \left\lfloor \frac{g_p N_G}{256} \right\rfloor + N_B^2 \times \left\lfloor \frac{b_p N_B}{256} \right\rfloor \quad (10)$$

where $\lfloor\ \rfloor$ is the integral operator.

3. Description of Proposed Approach

The procedures of the proposed coastline extraction approach include: (1) segmentation of a colour image, by using histogram analysis to decide the number of groups to which the colour image will be partitioned and by applying genetic algorithms to obtain an optimal fuzzy c-partition matrix, (2) interactive classification of the segmented image into water and land, (3) morphological filtering of the segmented image for noise removal, (4) delineation of coastlines from the filtered image, and (5) accuracy assessment by comparing the computer-extracted results with the manually digitized coastlines. Figure 1 shows the flowchart of the proposed approach.

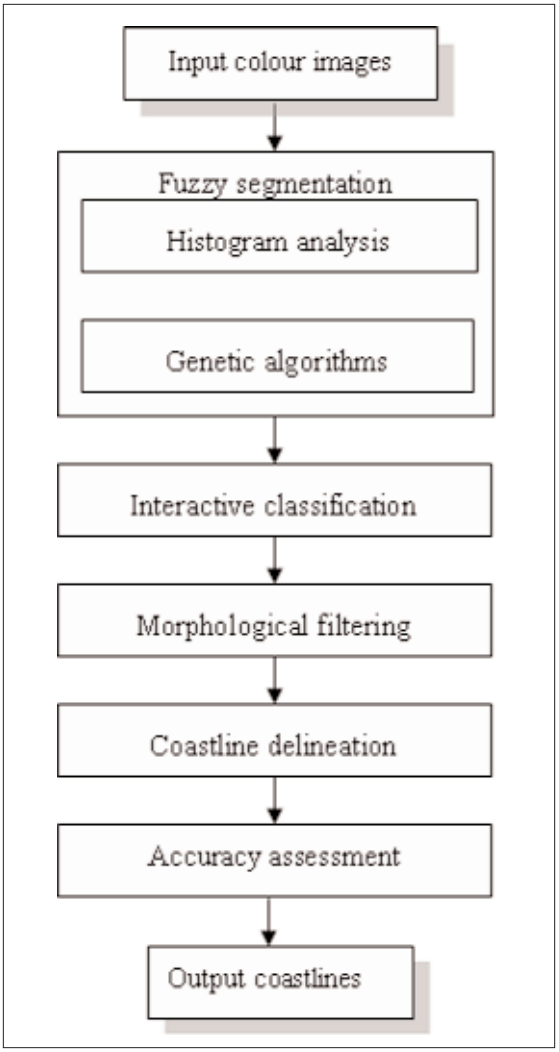

Figure: 1: Flowchart of the proposed approach.

3.1 Fuzzy Segmentation

Based on the concept of fuzzy c-partition mentioned above, a colour segmentation approach has been designed. The approach consists of three steps: (1) finding an initial centre vector set $\boldsymbol{CV}_0$, indicating the ranges in which the centre vectors are chosen in the following optimal procedure. This procedure is finished by using a histogram-based technique; (2) searching the best fuzzy c-partition using genetic algorithms to find an optimal fuzzy c-partition matrix; and (3) a defuzzifying procedure which converts the fuzzy c-partition matrix to the crisp c-partition matrix.

3.1.1 Pre-clustering

For the given colour image C, the colour histogram $H(C)$ can be obtained by the method described in Section 2.4. It is obvious that if the scene in a colour image is composed of distinct objects with different colours, its colour histogram usually shows peaks. Each peak corresponds to one object and adjacent peaks are likely to be separated by valleys. The height of a peak implies the number of pixels falling in the bin corresponding to the peak. The c highest peaks in the colour histogram can be detected, and the bins corresponding to the detected peaks determine the ranges in which the centre vectors are investigated for the purpose of optimization. The initial centre vectors are randomly selected from each of the c bins.

3.1.2 Optimizing

To search the optimal resolution of the fuzzy c-partition, genetic algorithms are utilized and designed as follows.

Chromosome Representation. The chromosome in a population is represented by a vector string consisting of c centre vectors corresponding to c clusters in a fuzzy c-partition. Figure 2 gives an example of such a string where $\boldsymbol{vc}$ denote the centre vectors.

Population Initialization. The initial population is created in such a way that the centre vectors in each chromosome are randomly chosen from the selected c bins. The number of chromosomes in a population (the length of population) is set as LP by the user, typically, $LP = 20 \sim 50$.

Fitness Computation. In order to use the genetic algorithm, it is necessary to define a fitness function. In this paper, the fitness of each chromosome in the population is evaluated as follows,

$$J_m(\boldsymbol{P},\boldsymbol{VC}) = \sum_{i=1}^{c}\sum_{j=1}^{n} P_{ij}\mu(\boldsymbol{v}_j, \boldsymbol{vc}_i) \qquad (11)$$

Genetic Operations. In this study, three kinds of genetic operators mentioned above are used to find the maximum value of J_m ($\boldsymbol{P,VC}$) [*Goldberg* 1989]. The conventional roulette wheel method is used for the selection operation; that is, the probability of selecting a chromosome is proportional to its fitness value. The one-point crossover is applied to two randomly selected chromosomes to generate their offspring. The crossover operation is applied stochastically with probability p_c, which implies that there are LP x p_c pairs of chromosomes chosen for the crossover operation. The mutation operation is carried out by replacing the chosen chromosome with a new chromosome. The mutation operation is performed with a fixed probability p_m, that is, LP x p_c chromosomes are selected for the operation.

Stop Criteria. The above genetic process is repeated until a terminating condition is reached. Commonly used terminating conditions [*Falkenauer* 1998] are (1) a found solution satisfying minimum criteria, (2) a fixed number of generations reached, (3) an allocated budget (computation time/money) reached, (4) the most ranking solution with fitness reaching a plateau so that successive iterations no longer produce better results, and (5) a visual inspection. In this study, the combination of (2) and (4) is used for the termination of generic algorithms.

3.1.3 Defuzzifying

In order to obtain the segmented image, transforming the fuzzy c-partition matrix to the crisp partition matrix is required, which can be done using the following defuzzification scheme.

After the best J_m ($\boldsymbol{P, VC}$) is found, let the relative $P = [p_{ij}]$ $i = 1, \ldots, c$ and $j = 1, \ldots, n$ be the fuzzy c-partition matrix, the percent partition matrix, p_p = [ppij] is defined as

$$p_{pij} = \frac{p_{ij}}{\sum_{j=1}^{n} p_{ij}} \qquad (12)$$

$\boldsymbol{vc}_1$	$\boldsymbol{vc}_2$	.....	$\boldsymbol{vc}_i$	.....	$\boldsymbol{vc}_c$

Figure 2: A chromosome consisting of c vectors.

where p_{ij} is the membership grade for pixel j belonging to cluster i. The crisp partition matrix, P_c = $[p_{cij}]$, is defined as

$$p_{cij} = \begin{cases} 1, & p_{pij} = \max_{i=1}^{c}\left(p_{pij}\right) \\ 0, & otherwise \end{cases} \qquad (13)$$

It is clear that each pixel in the crisp-partition matrix belongs to a certain cluster.

3.2 Interactive Classification and Morphological Filtering

We use interactive classification to group the segmented images into two object regions: land and water. Given the fact that noise (objects belong to neither land nor water) exists in the classified images, we use binary morphological operations for noise removal. For example, depending on the shape of noise objects, the appropriate combinations of binary closing or opening operators can be used to remove the noise (e.g. small islands out of the object area) or fill the holes within the object area, respectively.

3.3 Delineation

After extracting the water regions according to the colour features of water, an edge extraction algorithm is used to detect the skeletons of the detected water regions. To this end, a boundary extractor is designed and described in this section. Following the definition of 8-neighbourhoods shown in Figure 3, the boundary pixel of the water regions is determined if it is a contour pixel and satisfies the condition, $0 < N(p) < 8$, where $N(p)$ is the number of nonzero neighbours of pixel p, i.e.,

$$N(p) = \sum_{i=0}^{7} P_i \qquad (14)$$

4. Experimental Results

An experiment designed to demonstrate the performance of the proposed extraction approach was carried out on four test data sets, which are 1 m resolution IKONOS pan-sharpened images of four different scenes (see Figure 4, black-and-white images are used here). The size of each test image

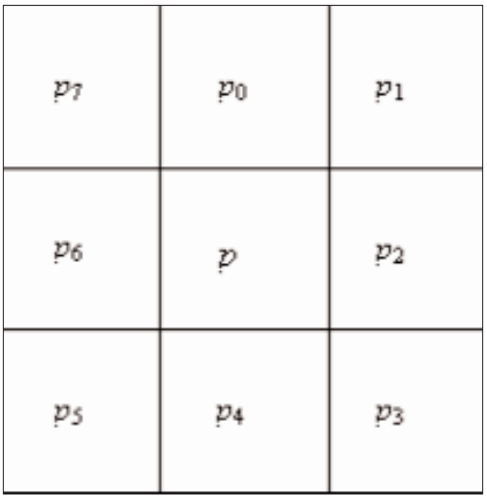

Figure 3: Neighbourhood arrangement.

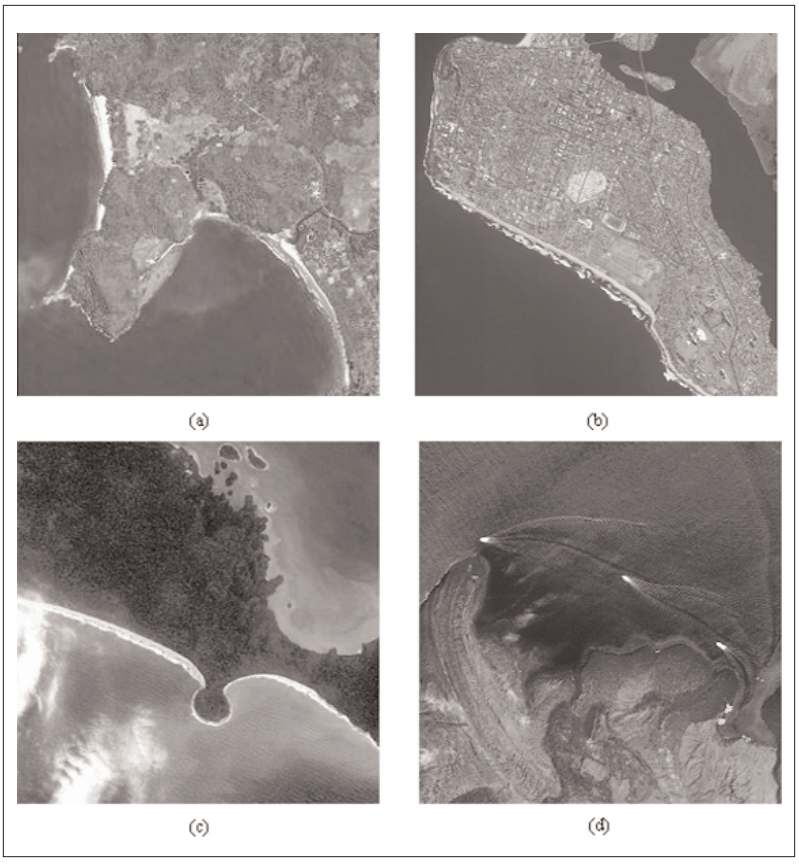

Figure 4: Four IKONOS test images of different scenes.

is 256 by 256 pixels. These images were geometrically rectified and projected to the UTM projection.

Figure 5 shows the histograms of the test images. The number of clusters was determined by analyzing these histograms. In this experiment, the number of intervals for discretizing each colour component was set at 8. As a result, a total of 512 (8^3) bins were obtained.

In order to obtain an appropriate number of clusters (regions) for segmentation, a threshold was set in advance. This means that those pixels in the corresponding bins will not be considered as an independent group during segmentation if values of the peaks in a histogram are less than the threshold. In practice, the threshold should be scene-dependent. For simplification, the threshold for all test images was set at 0.05. The numbers of peaks above the threshold are counted and considered to be the number of clusters. Table 1 lists the parameters used in the fuzzy segmentation algorithm which was applied to the test images. k_1 and k_2 are the parameters for calculating the colour similarity between two colour vectors.

Different combinations of these parameters were selected in this experiment and we found that the values of 0.0001 for k_1 and 0.2 for k_2 are suitable for segmentation of the test images. Considering the segmentation accuracy and computing time, the length of population (*Lp*) was chosen as 30. The maximum iteration (*Mi*) for stopping segmentation was set as 100. The experiment demonstrated that *Mi* was never reached when segmenting the four test images, since the segmentation algorithm converged to its stable state and stopped automatically before reaching *Mi*. In this study, the stable state of iterations is considered to be when the changes of fitness for the subsequent five iterations are less than 5%. The probabilities for crossover and mutation are taken as 0.2. That is, 6 chromosomes out of 30 chromosomes in the population are randomly selected to perform crossover and mutation operations, respectively.

Figure 6 shows the segmented images obtained by using the proposed segmentation algorithm (Note: black-and-white images are used here). By visual inspection of the segmented images, we can see that each test image has been partitioned into more than two classes. For example, as shown in Figure 6a, the areas in yellow white and pink dark-gray belong to water, while the areas in blue-black, green light gray and light black-red belong to land. By merging the yellow white and pink dark-gray areas, we obtain the land class (the black area shown in Figure 7a) and after merging the blackue, green light-gray and red light-black areas, we obtain the water class (the white area shown in Figure 7a). Figure 7 shows the binary images derived from the segmented images after the classification through a manually merging process.

As shown in Figure 7, smaller white areas exist in the land region (black), while smaller black areas exist in the water region (white), which are mainly caused by the radiation similarity of the water pixels to the land pixels and vice versa. In order to

eliminate those noise pixels, the binary morphological opening operator was applied on Figures 7a, 7b, and 7c to remove the smaller white areas (noise) appearing in the land region, while the closing operator on Figure 7d was used to remove the smaller black areas in the water region.

A 4X4 structuring element was used for both the opening and closing operators. Figure 8 shows the homogenous land regions (black) and water regions (white) after noise removal using the morphological filtering operations.

The boundaries between land (black) and water (white) were then extracted by the delineation algorithm described in Section 3.3. Figure 9 shows the delineated coastlines of the four test images.

5. Assessment and Discussions

Both visual inspection and buffer zone methods were used in this study for accuracy assessment. Figure 10 shows the extracted coastlines (red) overlaid on the original images. Visual inspection demonstrates that the extracted coastlines match the coastline images very well.

A buffer zone approach was also used for accuracy assessment in this study. The basic idea behind this approach is to calculate the distribution of the number of pixels of the extracted coastlines within a buffer zone around a reference coastline obtained by manual on-screen digitizing. The structure of the buffer on a given reference line B_0 (a set of pixels corresponding to the line) can be defined as:

$$b_i = \bigcup_{s \in B_{i-1}} N_s - B_{i-1} \tag{15}$$

where N_s is the 8 neighbour pixels located at s, b_i is the ith buffer layer, B_i is the union of all i buffer layers called i buffer, that is $B_i = \bigcup_{j=0}^{i} b_j$, $i = 1, 2, ...$

Figure 11 shows the buffer zone structure with two buffer layers, using the manually digitized line as the reference line (light gray).

The commission error (the black line shown in Figure 11) is defined as the ratio between the number of pixels on the computer-extracted line but out of the buffer zone for the manually digitized line and the total number of pixels of the computer-extracted line, i.e.

$$\mathrm{COM} = \frac{N_{EL} - N_{ELinMLB}}{N_{EL}} \tag{16}$$

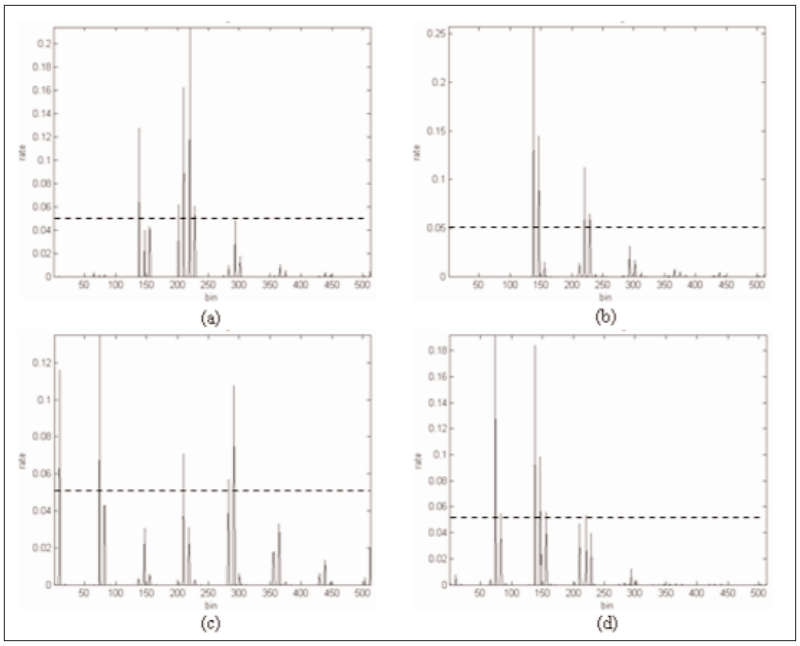

Figure 5: Histograms of the test images with threshold equal to 0.05.

Table 1. The parameters used in the segmentation process.

Parameters	(a)	(b)	(c)	(d)
k_1	0.0001	0.0001	0.0001	0.0001
k_2	0.2	0.2	0.2	0.2
c	5	5	4	6
m	2	2	2	2
Mi	100	100	100	100
Lp	30	30	30	30
p_c	0.2	0.2	0.2	0.2
p_m	0.2	0.2	0.2	0.2

where COM is the commission error, the black line segment shown in Figure 12, $N_{EL}in_{MLB}$ = #{{pixels ∈ manually digitized line buffer}∩{pixels ∈ computer extracted line}} and N_{EL} = #{pixels ∈ computer extracted line}.

The distribution probability of the computer extracted line on buffer layers for the manually digitized line can be calculated as follows:

$$pd(l) = \frac{N_{ELinFLB_1}}{N_{ML}} \tag{17}$$

where $l = 0, 1, 2 \ldots$, is the index of buffer layers, l = 0 is the manually digitized line, and $N_{ELinFLBl}$ =

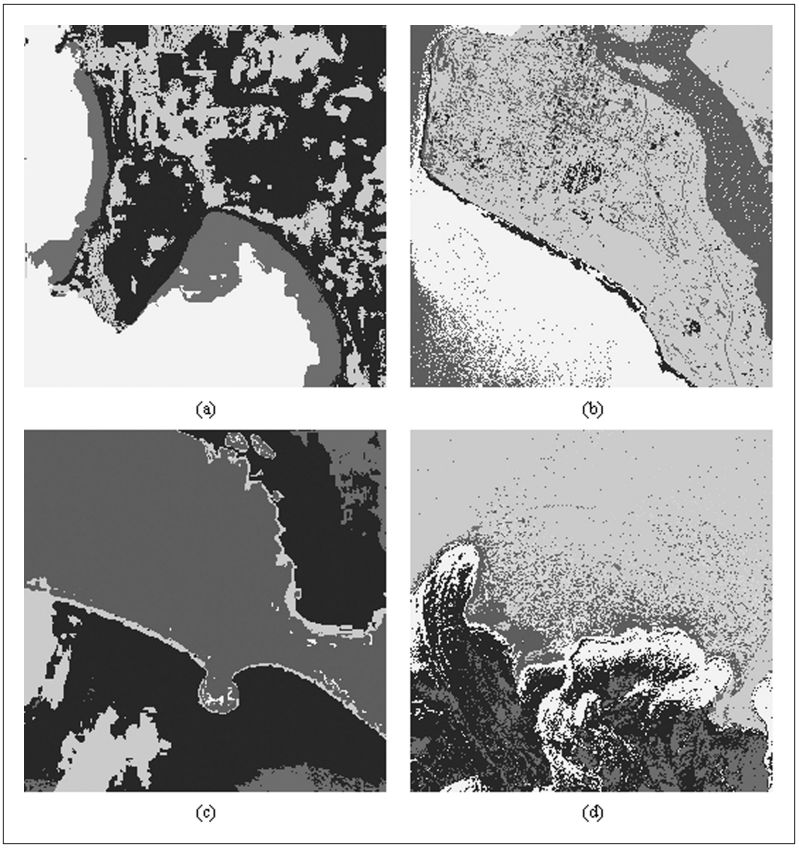

Figure 6: Segmented images.

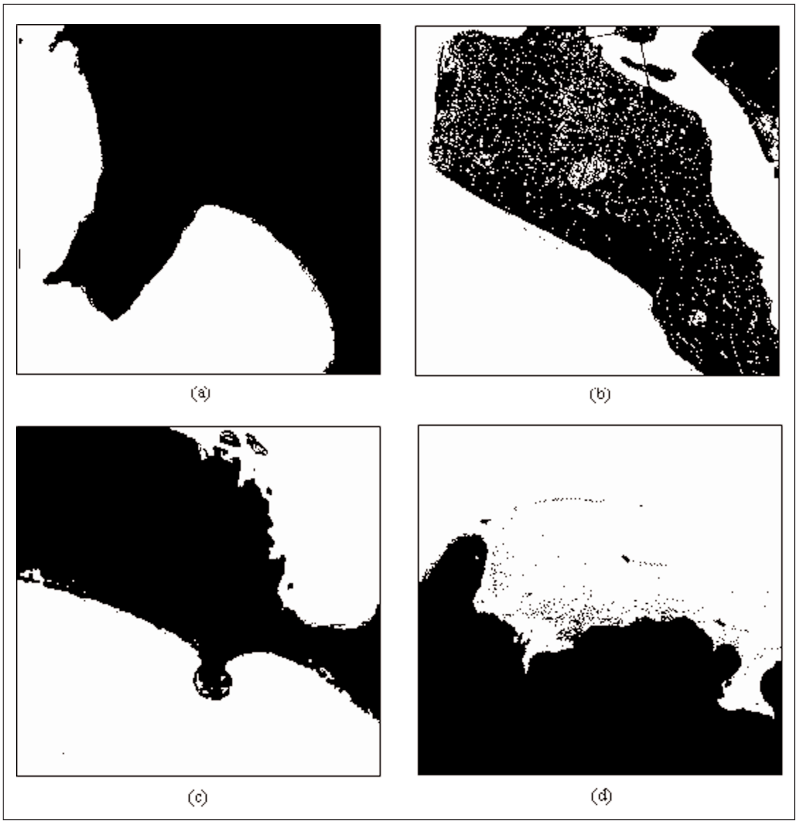

Figure 7: Classified images.

#{{pixels ∈ *l*th buffer layer}∩{pixels ∈ computer extracted line}}.

The cumulative probability of the extracted line on first *l* buffer layers is expressed as

(18)

$$pc(l) = \sum_{i=0}^{l} P(i)$$

The average error can be calculated from Equation 17, i.e.

$$AE = \sum_{l} l * pd(l) \qquad (19)$$

where the error *AE* is in units of a pixel.

The results of the extracted coastline using the proposed approach were evaluated according to the defined measurement. Figure 12 shows the distributed probabilities of the extracted coastline pixels within each buffer zone plotted against the cumulative probabilities calculated by Equations 17 and 18, respectively. In those curves, the probabilities corresponding to zero buffer zone imply the rates of the extracted coastline pixels coinciding with the reference coastline pixels.

As shown in Figure 12, the proposed approach exactly extracted more than 81 percent of the coastlines (on average). In the worst case d, more than 72% of the coastlines exactly extracted and more than 93% of the coastlines are extracted within one buffer zone of the reference costlines. Table 2 lists the commission errors and average errors calculated by Equations 16 and 19. It should be noted that the commission errors within the first three buffer zones (including zero buffer and first buffer) are considered in this evaluation.

As shown in Table 2, the average errors are less than one pixel and mean commission error is about 4.43% (≈(3.42+1.29+4.49+8.55) / 4). Both commission and average errors show that the proposed coastline extraction approach is both efficient and accurate.

Table 2. Commission errors and average errors.

Image	(a)	(b)	(c)	(d)
COM (%)	3.42	1.29	4.49	8.55
AE (pixels)	0.2	0.1	0.3	0.4

6. Conclusions

In this research, we present a new approach to automating coastline extraction from 1 m resolution IKONOS pan-sharpened imagery. Our approach uses a new fuzzy segmentation algorithm, which is based on the fuzzy c-partition and combines colour histogram analysis and generic algorithms. The segmentation process is fully automated since no initial coastline by manual selection is required. In our approach, the crucial step governing the positional accuracy of the extracted coastline is image segmentation. The accuracy of the image segmentation, in turn, depends on the reliability and correctness of the threshold. Our research represents a technical innovation to improve the accuracy and efficiency of the algorithms for achieving a reliable, optimal, and global threshold by combining colour histogram analysis and generic algorithms.

This approach was developed under the uniform image-processing framework and it does not require any auxiliary data from other sources, such as GIS databases. As a result, it can be easily completed and used with minimum human interaction. The developed approach was tested on four different test images and the extracted coastlines were evaluated by both visual inspection and buffer-zone methods. The experimental results show that the average errors are less than one pixel (0.2, 0.1, 0.3, and 0.4 pixels for the four test images, respectively) and mean commission error (under the accuracy of one pixel) is less than 4.4%.

Fully automated extraction of coastlines from high-spatial-resolution satellite images is a difficult and very challenging task because of the effects of ocean surface waves, coastal structures, shadows, low-intensity contrast between land and water regions, and other factors. Although our approach has demonstrated its accuracy and effectiveness, some further enhancements by considering shape and texture information could be made in a future version. Nevertheless, some human intervention may be inevitable in coastline extraction from very high-resolution satellite images, such as upcoming 0.4 m resolution GeoEye-1 and 0.25 m resolution GeoEye-2.

Acknowledgements

This research was partially supported by a Natural Sciences and Engineering Research Council of Canada (NSERC) discovery grant and the Public Safety Canada Research Fellowship. The authors would also like to thank the anonymous reviewers for their insightful critiques and constructive comments.

Figure 8: Filtered images.

Figure 9: Extracted coastlines.

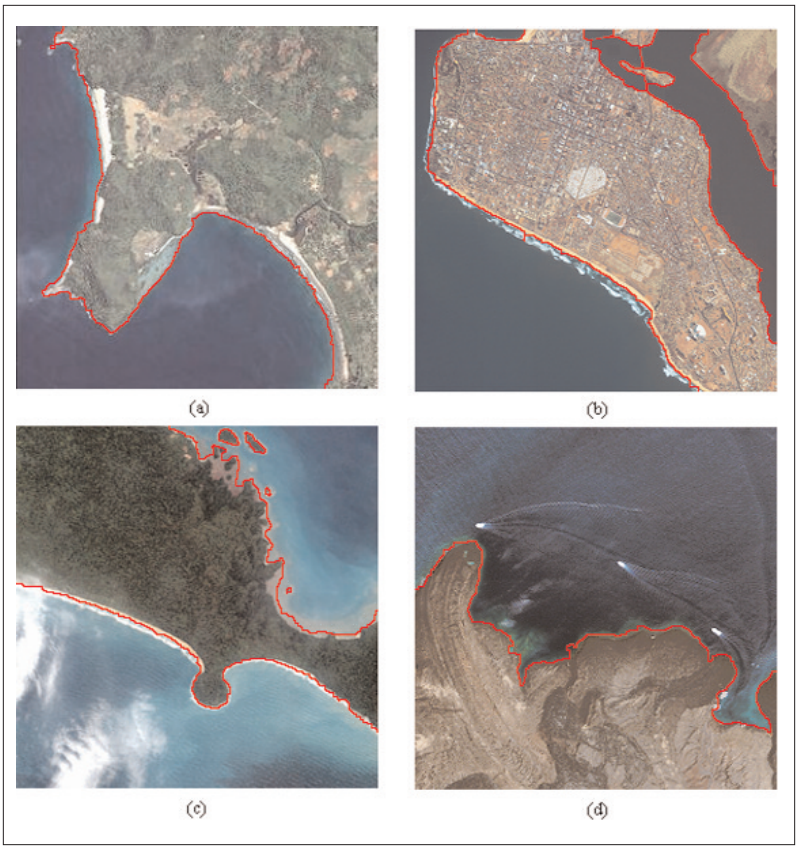

Figure 10: Extracted coastlines overlaid on original images.

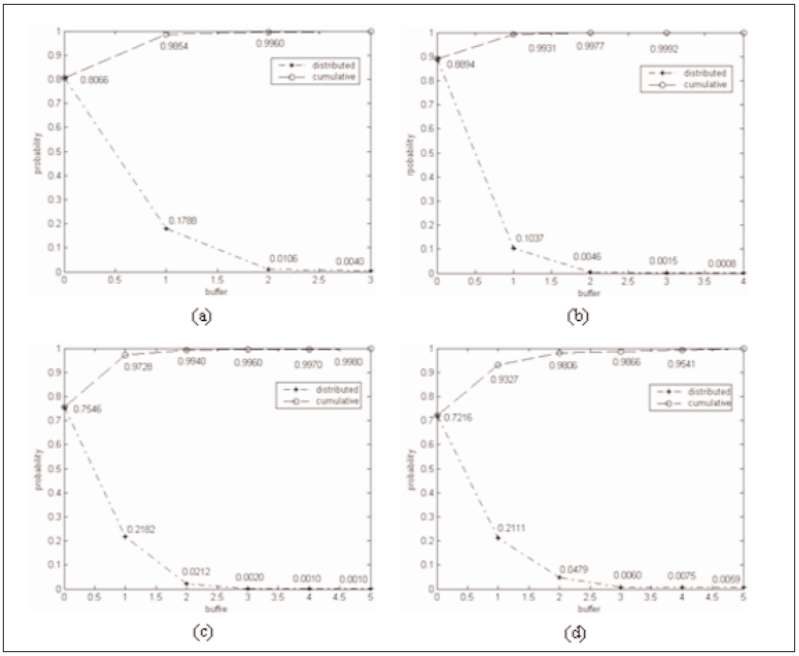

Figure 12: Probability distributions.

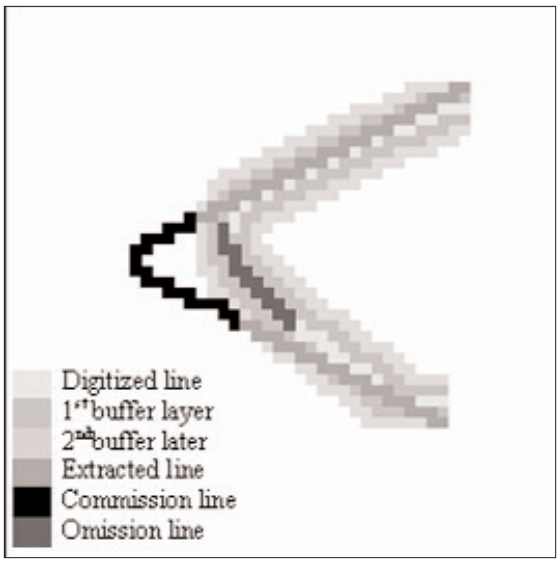

Figure 11: Buffer zone structure.

References

Colditz, R.R., T. Wehrmann, M. Bachmann, K. Steinnocher, M. Schmidt, G. Strunz and S. Dech. 2006. Influence of image fusion approaches on classification accuracy: A case study. *International Journal of Remote Sensing*, 27(15): 3311-3335.

Di, K., J. Wang, R. Ma and R. Li. 2003. Automatic shoreline extraction from high resolution IKONOS satellite imagery, *Proceedings of ASPRS 2003 Annual Conference*, May 2003, Anchorage, Alaska.

Falkenauer, E. 1998. *Genetic Algorithms and Grouping Problems*, Chichester: Wiley, 238 pp.

Green, D.R. and S.D. King (Eds.). 2003. *Coastal and Marine Geo-Information Systems - Applying the Technology to the Environment*, Berlin: Springer, 620 pp.

Goldberg, D.E. 1989. *Genetic Algorithms in Search, Optimization and Machine Learning*, Reading, MA: Addison-Wesley.

Heene, G. and S. Gautama. 2000. Optimisation of a coastline extraction algorithm for object-oriented matching of multisensor satellite imagery, *Proceedings of IGARSS* 2000, Honolulu, Hawaii, U.S., Vol. 6, pp. 2632-2634.

Klir, G. J. and B. Yuan. 1995. *Fuzzy Sets and Fuzzy Logic: Theory and Applications,* Upper Saddle River, New Jersey: Prentice Hall, 592 pp.

Li, J., Y. Li and M.A. Chapman. 2005. Small-format digital imaging for informal settlement mapping. *Photogrammetric Engineering & Remote Sensing*, 71(4): 435-442.

Li, R., K. Di and R. Ma. 2003. 3-D shoreline extraction from IKONOS satellite imagery. *Marine Geodesy*, 26(1):107-115.

Liu, H and K.C. Jezek. 2004. Automated extraction of coastline from satellite imagery by integrating Canny edge detection and locally adaptive thresholding methods, *International Journal of Remote Sensing*, 25(5): 937-958.

Marfai, M.A., H. Almohammad, S. Dey, B. Susanto and L. King. 2008. Coastal dynamic and shoreline mapping: multi-sources spatial data analysis in Semarang Indonesia. *Environmental Monitoring and Assessment*, 142: 297-308.

Polngam, S., T. Sanguantrakool, E. Pricharchon and S. Phoompanich. 2005. Remote sensing technology for tsunami disasters along the Andaman Sea, Thailand. *Proceedings of the 3rd International Workshop on Remote Sensing for Post-Disaster Response*, September 12-13, Chiba, Japan, pp. 1-16.

Pratt, W.K. 1991. *Digital Image Processing*, 2nd edition, New York: Wiley, 698 pp.

Ruiz, L.A., J.E. Pardo, J. Almonacid and B. Rodriguez. 2007. Coastline automated detection and multi-resolution evaluation using satellite images. *Proceedings of Coastal Zone 07*, Portland, Oregon, July 22-26, 5p.

Shapiro, L.G. and G.C. Stockman. 2001. *Computer Vision*, New Jersey: Prentice Hall.

Wang, Z., D. Ziou, C. Armenakis, D. Li and Q. Li. 2005. A comparative analysis of image fusion methods. *IEEE Transactions on Geoscience and Remote Sensing*, 43(6): 1391-1402.

Zhang, Y. 2004. Understanding image fusion. *Photogrammetric Engineering & Remote Sensing*, 70(6): 657-661.

Authors

Yu Li received his B.Eng. degree from XiDian University, Xian, China, in 1984 and his M.Sc. degree from Southeast University, Nanjing, China in 1991, both in electrical engineering. He was a Ph.D. candidate at Shanghai JiaoTong University, China, from 1998 to 2000. He obtained his M.A.Sc. degree in geomatics engineering from Ryerson University, Toronto, Ontario, in 2004. He is currently pursuing a Ph.D. degree in geomatics in the Department of Geography and Environmental Management, Faculty of the Environment at the University of Waterloo, Waterloo, Ontario. His current research interests include the development of spatial statistics algorithms for automated feature extraction from airborne LiDAR point clouds data, high-resolution aerial and spaceborne multispectral and SAR images.

Jonathan Li is Associate Professor of Geomatics, Department of Geography and Environmental Management at the University of Waterloo, Waterloo, Ontario. He received a Ph.D. degree in Geomatics Engineering from the University of Cape Town, South Africa. His career includes the position of Assistant Professor of Geomatics, Department of Geography at the University of Regina (2000-2001); Assistant Professor (2001-2004) and Associate Professor (2005-2006) of Geomatics Engineering, Department of Civil Engineering, Ryerson University, Toronto. He has co-edited 4 books and co-authored more than 100 research papers in refereed journals, books and conference proceedings. His current research interests include cartographic object extraction from image and range data, object-oriented classification techniques, and integrated geomatics solutions for disaster management. Dr. Li has served on the CIG Photogrammetry and National Committee for ISPRS since 2002. He is Chair of the ISPRS WG V/I on Land-based Mobile Mapping Systems (2008-2012) and Vice Chair of the ICA Commission on Mapping from Satellite Imagery (2008-2011).

Yao Lu received his B.Sc. degree in computer science from Shandong University, Jinan, China in 2005. He is currently pursuing a M.Sc. degree in geomatics in the Department of Geography and Environmental Management, Faculty of the Environment at the University of Waterloo, Waterloo, Ontario. His research work carried out at the Remote Sensing and Geospatial Technology Lab includes object-oriented feature extraction, land-use and land-cover classification, and change detection on the use of commercial high-resolution satellite imagery. ❑